Jurnal MIPA dan Pembelajarannya
e-issn: 2798-0634, email: jmipap.journal@um.ac.id

VOL	ISS	YEAR	DOI
6	3	2026	10.17977/um067.v6.i3.2026.2

A HYBRID METHOD BASED ON BLOCK-PULSE FUNCTIONS AND BERNOULLI POLYNOMIALS FOR THE EFFICIENT NUMERICAL SOLUTION OF TWO-DIMENSIONAL FRACTIONAL DIFFERENTIAL EQUATIONS

Mohammed Saleh Hadi

Mathmatical Department, Open Educational College, Wasit, Iraq
*Corresponding author, email: Mohammedhadi@ouwasit.edu.iq

Keywords
Two-Dimensional Fractional Differential Equations
Block-Pulse Function
Bernoulli Polynomials
Fractional Operational Matrices
Collocation Method

Abstract
The current paper is a new hybrid numerical approach to the solution of two-dimensional fractional differential equations (FDEs) based on Block-Pulse Functions (BPFs) and compact support as well as Bernoulli polynomials (BPs) with fast global convergence. The fractional differential equation is converted into a system of linear algebraic equations through the proposed method based on collocation methods at Gauss-Lobotto points, using operational matrices of fractional integral and derivative operators. The algorithm can be used with small bases ($M \leq 5$) to achieve high accuracy. The effectiveness of the method is confirmed by four numerical examples (including linear and nonlinear fractional differential equations) and a comparison with classical numerical methods. The approach is also used to a practical model to simulate the dispersion of the pollutants in the multi-layered soil systems. Findings indicate that hybrid approach provides a good compromise between computational cost and computational accuracy even with non-smooth solutions or complicated domains.

1. Introduction

Fractional differential equations (FDEs) have become an influential and essential mathematical tool to model complex systems with memory effects, hereditary behavior, and anomalous diffusion. Fractional operators, like the Riemann-Liouville integral and Caputo derivative, unlike their integer-order counterparts, have non-local kernels, which inherently represent long-range temporal and spatial interactions (Podlubny, 1999). This innate ability has seen the successful use of FDEs in a variety of fields in science such as modeling of viscoelastic materials (Oldham & Spanier, 1974), anomalous transport in porous media (Li & Zeng, 2015) and dynamics of a biological system (Mainardi, 1997). Although the theoretical basis of fractional calculus is well understood, the computational solution of FDEs, especially in multi-dimensional format, is still a major computation difficulty. The biggest challenge is that the fractional differential operators are not local, and therefore, the solution value at any point is determined by the whole past history or spatial range. As a result, classical numerical techniques such as finite differences when used in a naive form, result in dense algebraic systems with computational complexity and storage requirements that increase prohibitively with the refinement of the discretization (Bhrawy & Alghamdi, 2014). This non-locality curse requires one to devise special, high-order algorithms capable of attaining spectral accuracy whilst controlling computational cost. To address this difficulty, orthogonal-polynomial spectral and pseudo-spectral methods (e.g., Chebyshev, Legendre, Bernoulli) have become popular in the solution of one-dimensional FDEs. These techniques take advantage of the international smoothness of functions to have exponential convergence of sufficiently smooth solutions (Doha et al., 2011). However, their direct extension to problems with weak singularities or in complex geometries can be problematic. In contrast, piecewise basis functions, including Block-Pulse Functions (BPFs), are highly localized and produce sparse operation matrices since they have compact support and thus are computationally efficient in problems with sharp gradients or discontinuities (Saadatmandi & Dehghan, 2010). However, they normally only give algebraic convergence rates. One potential

approach to the complementary advantages of both methods is to build hybrid basis functions. The first successful study by Diethelm (2010) showed the effectiveness of combining BPFs with Bernoulli polynomials (BPs) to one-dimensional fractional PDEs. The hybrid basis has the local approximation property of BPFs, and the high-order convergence of BPs. More recent developments have also delved into such hybrid schemes of integral equations and fractional models in applied sciences (Garrappa, 2018; Zayernouri & Karniadakis, 2013). Even with these developments, an effective and generalizable theory of two-dimensional FDEs in a BPF-Bernoulli hybrid basis, with a detailed analysis of the working matrices and convergence behaviour, is not yet comprehensively developed in the literature. To fill in this gap, the present paper suggests a new and systematic hybrid spectral-collocation algorithm to numerically solve a two-dimensional FDE. The following are our major contributions: We use the one-dimensional BPF-Bernoulli bases to build a two-dimensional hybrid basis and compute the operational matrices of the Riemann-Liouville fractional integral and Caputo derivative in two dimensions. Our method of discretizing the FDE uses a collocation method at Gauss-Lobotto nodes, converting it into a well-posed, sparse linear equation. This methodology greatly lowers the computational aspect as opposed to global spectral methods. We theoretically analyze convergence of the method, give error bounds, which are a product of the piecewise and the polynomials component of the basis. We confirm the high accuracy and computational efficiency of the method by extensive numerical tests of benchmark problems, such as linear and nonlinear two-dimensional FDEs. We illustrate the usefulness of the method in practice by putting it into practice on a model of anomalous dispersion of pollutants in a multi-layered soil system, an application of modern and contemporary importance in environmental engineering (Meerschaert & Tadjeran, 2006; Benson et al., 2000).

The rest of this paper is structured as follows: Section 2 discusses necessary definitions in terms of fractional calculus, and the properties of BPFs and Bernoulli polynomials. Part 3 describes the development of the hybrid basis and the derivalge of the essential working matrices. Section 4 gives the collocation scheme of two-dimensional FDEs. Section 5 presents a convergence analysis. Numerical results and comparisons are reported in Section 6. In Section 7, a practical application is presented. Lastly, Section 8 wraps up the paper and proposes future research directions.

2. Method

2.1. Mathematical Fundamentals

This section provides the essential theoretical framework for the proposed hybrid method. We present the core definitions of fractional calculus in the Riemann-Liouville and Caputo senses, followed by the definitions and key properties of the two basis function families: Block-Pulse Functions and Bernoulli polynomials.

2.1.1. Fractional Calculus

Fractional calculus generalizes the concepts of differentiation and integration to arbitrary (non-integer) orders. We employ the following standard definitions (Mainardi, 1997; Podlubny, 1999).

Definition 2.1. (Riemann-Liouville Fractional Integral)

Let $f \in L^1([a,t])$ and $\alpha > 0$. The left-sided Riemann-Liovuille fractional integral of order α is defined as:

$$I_{a+}^{\alpha} f(t) = \frac{1}{\Gamma(\alpha)} \int_a^t (t-\tau)^{\alpha-1} f(\tau) d\tau, \qquad t > a \tag{1}$$

Where $\Gamma(\cdot)$ is the Euler gamma function. For simplicity and without loss of generality, we set $a = 0$ and denote $I^{\alpha} f(t) \equiv I_{0+}^{\alpha} f(t)$.

Definition 2.2. (Caputo Fractional Derivative)

Let $m = \lceil \alpha \rceil$ be the smallest integer greater than or equal to $\alpha > 0$, and assume $f \in C^m([a,T])$. The Caputo fractional derivative of order α is defined as:

$$D_{a+}^{\alpha} f(t) = I_{a+}^{m-\alpha} D_t^m f(t) = \frac{1}{\Gamma(m-\alpha)} \int_a^t (t-\tau)^{m-\alpha-1} f^m(\tau) d\tau, \tag{2}$$

Where D_t^m denotes the classical m-th order derivative. This definition is particularly favored in initial value problems because it allows the imposition of standard initial conditions in the form of

integer-order derivatives, i.e., $f^{(k)}(a), k = 0,1, \ldots, m-1$ (Podlubny, 1999). As with the integral, we set $a = 0$ and use D^{α}.

2.1.2. Block-Pulse Functions (BPFs)

Block-pulse functions form a complete, orthogonal set of piecewise constant basis functions define on partitioned interval offering excellent local representation (Oldham & Spanier, 1974; Saadatmandi & Dehghan, 2010).

Definition 2.3. (BPF Set)

For a fixed positive integer m, partition the interval $[0, T]$ into m equal subintervals of width $h = T/m$. The $i-th$ Block-pulse function $\psi_i(t)$, for $i = 1,2, \ldots, m$, is defined as:

$$\psi_i(t) = \begin{cases} 1, & t \in [(i-1)h, ih) \\ 0, & otherwise \end{cases} \quad (3)$$

Property 2.1 (Orthogonality)

The BPFs are orthogonal in the standard L^2 sense with the inner product on $[0, T)$:

$$\int_0^T \psi_i(t)\psi_j(t)\, dt = h\delta_{ij}, \quad (4)$$

Where δ_{ij} is the Kronecker delta. This property leads to diagonal system matrices when representing multiplicative operations, contributing to computational sparsity.

Property 2.2 (Completeness)

The set $\{\psi_i(t)\}_{i=1}^m$ is complete in $L^2[0, T)$ (Jin et al., 2021). Any function $f(t) \in L^2[0, T)$ can be approximated as:

$$f(t) \approx \sum_{i=1}^m f_i \psi_i(t), \quad (5)$$

Where f_i is typically taken as the average value of $f(t)$ on the i-th subinterval, i.e.,

$f_i = \frac{1}{h}\int_{(i-1)h}^{ih} f(t)dt$. The L^2-error of this approximation converges to zero as $m \to \infty$.

2.1.3. Bernoulli polynomials

Bernoulli polynomials constitute a sequence of polynomials that can be orthogonalized on the interval [0,1] known for their smoothness and rapid convergence properties when approximating sufficiently regular functions (Garrappa, 2018; Li & Zeng, 2015).

Definition 2.3.1. (Bernoulli polynomials)

The Bernoulli polynomials $B_n(t)$,$n \in N_0$, can be define via their exponential generating function:

$$\frac{xe^{tx}}{e^x - 1} = \sum_{n=0}^{\infty} B_n(t)\frac{x^n}{n!}, \ |x| < 2\pi. \quad (6)$$

The first few polynomials are: $B_0(t) = 1$,$B_1(t) = t - \frac{1}{2}$,$B_2(t) = t^2 - t + \frac{1}{6}$.

Property 2.3 (Orthogonality on [0, 1])

While not orthogonal in the standard L^2 sense, shifted Bernoulli polynomials can be orthogonalized. A set of orthonormal Bernoulli polynomials $\hat{B}_n(t)$ on [0,1] can be constructed via the Gram-Schmidt process from the monomial basis $\{1, t, t^2, \ldots\}$.

They satisfy: $\int_0^1 \hat{B}_i(t)\hat{B}_j(t)dt = \delta_{ij}$.

In practice, the original polynomials $B_n(t)$ are often used for their simple explicit form, and their quasi-orhogonality is managed within the numerical scheme.

Property 2.4 (Differentiation and Integration)

Bernoulli polynomials satisfy simple differentiation rules: $\grave{B}_n(t) = nB_{n-1}(t)$.

Furthermore, their integrals over [0,1] vanish for $n \geq 1$: $\int_0^1 B_n(t)dt = 0$.

These properties facilitate the construction of operational matrices for differential and integral operators.

2.2. Hybrid Basis and Operational Matrices

2.2.1. Hybrid Basis Functions:

The cornerstone of the proposed numerical scheme is the construction of a hybrid basis that synergistically merges the complementary attributes of Block-pulse Functions (BPFs) and Bernoulli polynomials (BPs). For the one-dimensional case on the interval [0,T) partitioned into m subinterval of width $h = {}^{T}/_{m}$, we define the hybrid basis functions $\phi_{ij}(t)$ as product of locally supported BPF and globally smooth BP, specifically:

$$\phi_{ij}(t) = \psi_i(t)B_j\left(\frac{t-(i-1)h}{h}\right), i = 1, \dots, m, \quad j = 0, \dots, n,$$

Where $\psi_i(t)$ is the i-th BPF from definition 2.3, and $B_j(\xi)$ is the j-th Bernoulli polynomial mapped to the local coordinate $\xi \in [0,1]$ on the i-th subinterval. This construction ensures that $\phi_{ij}(t)$ is supported exclusively on $[(i-1)h, ih)$, inheriting the sparsity and localization of BPFs. Simultaneously, within this support, it replicates the excellent approximation capabilities and high-order smoothness of the Bernoulli polynomial B_j. Consequently, any function $u(t) \in L^2([0,T))$ can be approximated as:

$$u(t) \approx u_m^n(t) = \sum_{i=1}^{m}\sum_{j=0}^{n} c_{ij}\phi_{ij}(t) = C^T\Phi(t),$$

Where $C = [c_{10}, \dots, c_{mn}]^T$ is the vector of unknown coefficients and $\Phi(t)$ is the corresponding vector of hybrid basis functions. The extension to two dimensions for the domain $[0, T_x) \times [0, T_y)$ is achieved via a standard tensor product construction, yielding the 2D hybrid basis:

$$\Phi_{ijkl}(x,y) = \phi_{ij}^{(x)}(x)\phi_{kl}^{(y)}(y) = \psi_i^{(x)}(x)B_j\left(\frac{x-(i-1)h_x}{h_x}\right)\psi_k^{(y)}(y)B_l\left(\frac{y-(k-1)h_y}{h_y}\right),$$

Where $\phi_i^{(x)}$and $\phi_k^{(y)}$are the 1D hybrid bases in the x-and y-directions, respectively, with corresponding partitions m_x, m_y and polynomial degrees n_x, n_y. This tensor product basis retains the desired properties: the support of each 2D basis function is the rectangular subdomain $[(i-1)h_x, ih_x) \times [(k-1)h_y, kh_y)$, sparsity of the matrix, and the high-order approximation of the solution within each element is made possible by components of the polynomials. It is a type of hybrid framework which is well-suited to the non-local nature of the operators of, and the spectral accuracy of, global high-order polynomials, so it is especially suitable to the non-local operators and potential solution singularities of a fractional differential equation. Further derivation of operational matrices of fractional integration and differentiation are directly based on this closely-grown hybrid basis.

2.2.2. Operational Matrix for Fractional Integration

A pivotal element of the proposed hybrid method is the construction of an operational matrix for the Riemann-Liouville fractional integral associated with the hybrid basis $\Phi(t)$. Let I^α denote the fractional integral operator of order $\alpha > 0$ as given in definition 2.1. Applying this operator to the vector of hybrid basis functions yields a new vector function. Because the set $\{\phi_{ij}(t)\}$ spans a finite-dimensional subspace, the image $I^\alpha\phi_{ij}(t)$ can be expanded again in terms of the same basis with a high degree of accuracy. This leads to the following matrix representation.

Definition 3.1 (Fractional Integration Operational Matrix)

The fractional integration operational matrix of order α, denoted by

$P^\alpha \in \mathbb{R}^{(m(n+1)\times(m(n+1))}$ is defined by the relation

$I^{\alpha}\Phi(t) \approx P^{\alpha}\Phi(t), \quad t \in [0,T),$

Where$\Phi(t) = [\phi_{10}(t), \dots, \phi_{1n(}(t), \dots, \phi_{m0}(t), \dots, \phi_{mn(t)}]^{T}.$

To determine the entries of P^{α}, we exploit the piecewise nature of hybrid basis. For a fixed pair (i,j) the basis function $\phi_{ij}(t)$ is supported only on the subinterval $(i-1)h, ih)$ with $h = {}^{T}/_{m}$. Consequently, its fractional integral $I^{\alpha}\phi_{ij}(t)$ is identically zero for $t < (i-1)h$. For $t \geq (i-1)h$, we write

$$I^{\alpha}\phi_{ij}(t) = \frac{1}{\Gamma(\alpha)}\int_0^t (t-\tau)^{\alpha-1}\,\phi_{ij}(\tau)d\tau = \frac{1}{\Gamma(\alpha)}\int_{(i-1)h}^{\min(t,ih)} (t-\tau)^{\alpha-1} B_j\left(\frac{\tau-(i-1)h}{h}\right)d\tau.$$

When t belongs to the k-th subinterval, i.e. $t \in [(k-1)h, kh)$ with $k \geq i$, we split the integration interval and change variable $\xi = (\tau-(i-1)h)/h$ to obtain a closed form. The resulting expression involves incomplete Beta functions or, more conveniently, a finite series representation using the binomial expansion of $(t-\tau)^{\alpha-1}$.

Lemma 3.1 (Explicit expression for the fractional integral of a hybrid basis function)

For $t \in [(k-1)h, kh)$ with $k \geq i$, let $\hat{t} = t-(i-1)h$. Define the translated and scaled variable $\eta_k = \hat{t}/h - (k-i)$. Then

$$I^{\alpha}\phi_{ij}(t) = \frac{h^{\alpha}}{\Gamma(\alpha)}\sum_{r=0}^{\infty}\binom{\alpha-1}{r}(-1)^r \eta_k^{\alpha-1-r}\int_{\max(0,\eta_k-1)}^{\eta_k}\xi^r B_j(\xi)d\xi,$$

Where the integral of $\xi^r B_j(\xi)$ can be evaluated exactly as polynomial in η_k.

In practice, because B_j is a polynomial of degree j, the integral reduces to a finite combination of power of η_k.

Proof.

Substitute $\tau = (i-1)h + h\xi$ into the integral representation. Then

$$I^{\alpha}\phi_{ij}(t) = \frac{h^{\alpha}}{\Gamma(\alpha)}\int_0^{\eta_k}(\eta_k-\xi)^{\alpha-1}B_j(\xi)d\xi,$$

With $\eta_k = (t-(i-1)h)/h$. Expand $(\eta_k-\xi)^{\alpha-1}$ using the generalized binomial series: $(\eta_k-\xi)^{\alpha-1} = \sum_{r=0}^{\infty}\binom{\alpha-1}{r}{\eta_k}^{\alpha-1-r}(-\xi)^r$.

Term wise integration yields the stated formula. The series terminates if α is an integer, otherwise it is infinite series that converges absolutely for $0 \leq \xi \leq \eta_k$and can be truncated to desired accuracy.

3.3. Operational Matrix for Fractional Differentiation

Based on the fractional integration derived operational matrix in the preceding subsection we now create the operational matrix of the Caputo fractional derivative. This is the matrix required in the discretization of the fractional differential equations in which the derivative term is known explicitly. The construction uses the basic connection between the Caputo derivative and the Riemann-Liouville integral and the classical differentiation operators on a mixed basis.

Recall that Caputo fractional derivative of order $\alpha > 0$ is defined for a sufficiently smooth function $f(t)$ as:

$$D^{\alpha}f(t) = I^{m-\alpha}f^{(m)}(t)\,, m = [\alpha]\,,$$

Where $f^{(m)}(t)$ denotes the classical m-th order derivative. This definition provides a direct pathway to construct the operational matrix:

First, differentiate the basis functions classically, and then apply the fractional integral operator of order $m-\alpha$.

Definition 3.2 (Fractional Differentiation Operational Matrix)

The Caputo fractional differentiation operational matrix of order $\alpha > 0$ denoted by $D^{\alpha} \in R^{(m(n+1))\times(m(n+1))}$, is defined by the relation

$$D^{\alpha}\Phi(t) \approx D^{\alpha}\Phi(t) \quad , \ t \in [0,T),$$

Where $\Phi(t)$ is the vector of hybrid basis function

To determine the entries of D^{α}, we proceed in two stages. First, we compute the classical derivative of each hybrid basis function. Second, we expand the result in the hybrid basis and apply the fractional integration matrix $P^{m-\alpha}$. The following lemma provides the essential building block.

Lemma 3.2 (Classical derivative of a hybrid basis function)

For a fixed pair (i,j) with $i \in \{1,\dots,m\}$ and $j \in \{0,\dots,n\}$, the classical derivative of the hybrid basis function $\phi_{ij}(t)$ is given by

$$\frac{d}{dt}\phi_{ij}(t) = \psi_i(t)\frac{1}{h}\grave{B}_j\left(\frac{t-(i-1)h}{h}\right) + \delta(t-(i-1)h)B_j(0) - \delta(t-ih)B_j(1),$$

Where $\delta(\cdot)$ denotes the Dirac delta distribution, and $\grave{B}_j(\xi) = jB_{j-1}(\xi)$ is the derivative of the Bernoulli polynomial. The terms involving Dirac deltas arise from the discontinuities of $\psi_i(t)$ at the subinterval boundaries.

Proof

The hybrid basis function $\phi_{ij}(t)$ is the product of the piecewise constant BPF $\psi_i(t)$ and the Bernoulli polynomial B_j evaluated at the scaled local coordinate $\xi(t) = (t-(i-1)h)/h$. On the open interval $((i-1)h, ih)$, $\psi_i = 1$, so the derivative exists in the classical sense and is given by the chain rule:

$$\frac{d}{dt}\psi_i(t) = \delta(t-(i-1)h) - \delta(t-ih)\,.$$

Applying the product rule for distributions,

$$\frac{d}{dt}\phi_{ij}(t) = \left(\frac{d}{dt}\psi_i(t)\right)B_j\big(\xi(t)\big) + \psi_i(t)\frac{d}{dt}B_j\big(\xi(t)\big).$$

Substituting the expressions yields the stated result.

To construct a numerical scheme that avoids dealing with distributions, we work in a weak (integral) formulation. When the Caputo derivative is applied, the distributional terms are integrated against sufficiently smooth test functions, and their effect is captured through the boundary conditions of the problem. In practice, when using a Galerkin or collocation method, we can avoid explicit handling of the delta functions by first applying the fractional integral operator to the classical derivative, as shown below.

Theorem 3.1 (construction of the fractional differentiation matrix)

Let P^{β} be the fractional integration operational matrix of order $\beta = m - \alpha$ from definition 3.1. Let Q be the matrix representing the classical m-th derivative operator in the hybrid basis,

$$\frac{d^m}{dt^m}\Phi(t) \approx Q\Phi(t)\,.$$

Then the Caputo fractional differentiation operational matrix of order α is given by

$$D^{\alpha} = P^{m-\alpha}Q.$$

Proof

For any function $u(t)$ approximated as $u(t) = C^T\Phi(t)$, we have

$$D^{\alpha}u(t) = I^{m-\alpha}u^{(m)}(t) \approx I^{m-\alpha}\big(C^TQ\Phi(t)\big) \approx C^TQI^{m-\alpha}\Phi(t) \approx C^TQP^{m-\alpha}\Phi(t).$$

Since the left-hand side should be representable as $C^T D^\alpha \Phi(t)$ by the definition, the matrix D^α must satisfy $D^\alpha = QP^{m-\alpha}$ when acting on the coefficient vector from the right. However because matrix multiplication is associative, we can define the operational matrix for the derivative as acting on the basis functions themselves, yielding $D^\alpha = P^{m-\alpha}Q$. The order of multiplication reflects whether we consider the operator acting on the coefficient vector or on the basis functions; both conventions are equivalent up to transposition. In the standard Galerkin framework where we expand the solution and test against the basis, the form $D^\alpha = P^{m-\alpha}Q$ is appropriate.

The matrix Q for classical m-th derivative is constructed using the polynomial nature of the Bernoulli component. Within each subinterval, the derivative of a Bernoulli polynomial is another Bernoulli polynomial of lower degree, as per property 2.4. Specifically,

$$\frac{d^m}{dt^m} B_j\left(\frac{t-(i-1)h}{h}\right) = \begin{cases} \frac{j!}{(j-m)!} h^{-m} B_{j-m}\left(\frac{t-(1-i)h}{h}\right), & j \geq m, \\ 0, & j < m\,. \end{cases}$$

Thus, the action of d^m/dt^m on hybrid basis remains within the span of the hybrid functions, but possibly with a reduced polynomial degree. The matrix Q is therefore block-diagonal, with each block corresponding to subinterval, and within each block, it is upper-triangular (vanishing for low-degree polynomials). This arrangement,together with the block-lower-triangularity of P(m-α), means that D with α inherits a desirable sparsity structure, so that the resulting linear systems can be solved efficiently using iterative methods.

To conclude, the fractional differentiation operation matrix D alpha is the product of the fractional integration matrix of the m-alpha order and the classical differentiation matrix of the m order.. This construction is both mathematically rigorous and computationally convenient, as it leverages precomputed components and preserves the sparsity essential for large-scale simulations of two-dimensional fractional differential equations.

2.3. Collocation Method for Two-Dimensional Fractional Differential Equations

2.3.1. Problem Formulation

We consider the two-dimensional fractional differential equation of mixed order on the unit square domain $\omega = [0,1] \times [0,1]$ in the general form:

$$D_x^\alpha u(x,y) + D_y^\beta u(x,y) = f(x,y) \quad , (x,y) \in \omega,$$

Supplemented with appropriate boundary conditions (Mainardi, 1997; Podlubny, 1999). Here D_x^α, D_y^β denote the Caputo fractional derivatives of order $\alpha, \beta \in (0,1)$ (or $\alpha, \beta \in (1,2)$ depending on the nature of the problem) with respect to the variables x and y, respectively, and the function $f(x,y)$ is known. This model represents a wide class of physical and engineering problems, including pollutant dispersion and anomalous diffusion in porous media (Bhrawy & Alghamdi, 2014; Zayernouri & Karniadakis, 2013).

2.3.2. Solution approximation using the Two-Dimensional Hybrid Basis

We construct the two-dimensional hybrid basis using the tensor product of the one-dimensional hybrid basis define in Section 3.1. Let m_x, m_y be the numbers of Block-pulse Functions in the x and y directions, respectively, and n_x, n_y the maximum degrees of Bernoulli polynomials we define the two-dimensional hybrid basis functions as follows:

$$\Phi_{ijkl}(x,y) = \phi_{ij}^{(x)}(x)\phi_{ij}^{(y)}(y), \quad i,k = 1,\dots,m, \quad j,l = 0,\dots,n,$$

Where $\phi_{ij}^{(x)}(x)$ the hybrid basis are functions in the x-direction defined by:

$$\phi_{ij}^{(x)}(x) = \psi_i(x) B_j\left(\tfrac{x-(i-1)h_x}{h_x}\right), \qquad h_x = \tfrac{1}{m_x},$$

Similarly for $\phi_{kl}^{(y)}(y)$. These basis functions are supported on the sub-rectangles $[(i-1)h_x, ih_x) \times [(k-1)h_y, kh_y)$, ensuring the structural sparsity of the resulting matrices (Oldham & Spanier, 1974; Saadatmandi & Dehghan, 2010).

We approximate the solution $u(x,y)$ as:

$$u(x,y) \approx u_{m,n}(x,y) = \sum_{i=1}^{m_x}\sum_{j=0}^{n_x}\sum_{k=1}^{m_y}\sum_{l=0}^{n_y} c_{ijkl}\Phi_{ijkl}(x,y) = C^T\Phi(x,y),$$

Where C is the vector of unknown coefficients of length $N = m_x(n_x+1)\cdot m_y(n_y+1)$, and $\Phi(x,y)$ is the vector of basis functions.

2.3.3. Application of the Collocation Method

The collocation method relies on enforcing the differential equation to be satisfied at selected points within the domain, called collocation points (Diethelm, 2010; Doha et al., 2011; Oldham & Spanier, 1974). We choose the collocation points (x_p, y_q) as follows:

1. Let $\{x_{i,r}\}_{r=0}^{n_x}$ be the Gauss-Lobatto points on the i-th subinterval after scaling from [0,1] to $[(i-1)h_x, ih_{x)}$, and similarly $\{y_{k,s}\}_{s=0}^{n_y}$ on the k-th subinterval.
2. We apply the fractional derivative to the approximation (4.3) using the operational matrices derived in Section 3.3. for the x-direction, we have:

$$D_x^\alpha u(x,y) \approx \sum_{i=1}^{m_x}\sum_{j=0}^{n_x}\sum_{k=1}^{m_y}\sum_{l=0}^{n_y} c_{ijkl}\left(D_x^\alpha \phi_{ij}^{(x)}(x)\right)\phi_{kl}(y) = C^T(D_x^\alpha \quad I_y)\Phi(x,y),$$

Where D_x^α is the fractional differentiation matrix in the x-direction (of dimension $m_x(n_x+1)\times m_x(n_x+1)$) and I_y is the identity matrix in the y-direction (of dimension $m_y(n_y+1)\times m_y(n_y+1)$), and $\otimes$ denotes the Kronecker product (Li & Zeng, 2015). Similarly for the y-direction.

$$D_y^\beta u(x,y) \approx C^T\left(I_x \otimes D_y^\beta\right)\Phi(x,y).$$

Substituting these representations into equation (4.1) and collocating at the points (x_p, y_q) we obtain:

$$C^T\left[\left(D_X^\alpha \otimes I_y\right)\Phi(x,y) + \left(I_x \otimes D_y^\beta\right)\Phi\left(x_p, y_q\right)\right] = f\left(x_p, y_q\right),$$

For each $p = 1, \dots, m_x(n_x+1)$ and $q = 1, \dots, m_y(n_y+1)$.

2.3.4. The Linear Algebraic system

We write the above equations in the form of a linear algebraic system. Define the system matrix A as:

$$A = \left(D_X^\alpha \otimes I_y\right) + \left(I_x \otimes D_y^\beta\right) \in R^{N\times N},$$

Moreover, define the right-hand side vector F where:

$$F_{p,q} = f\left(x_p, y_q\right), \quad p,q = 1, \dots, \sqrt{N},$$

Rearranging the indices lexicographically (Li & Zeng, 2015; Podlubny, 1999), we obtain the system:

Ac =f,

Where c the vector of unknown coefficient and f is is the vector of function values f at the collocation points.

Theorem 4.1 (Solvability).

If D_x^α and D_y^β are non-singular matrices, then the system matrix A is invertible, and thus there exists a unique solution $c = A^{-1}$f.

Proof

The matrices D_x^{α} and D_y^{β} are based on orthogonal basis sets, making then full-rank matrices. The Kronecker product of two full-rank matrices yields a full-rank matrix (Li & Zeng, 2015). The inevitability of A depends on spectral properties and cannot be guaranteed solely by rank arguments (Oldham & Spanier, 1974). However, under appropriate collocation and boundary enforcement A is observed to be well conditioned (Saadatmandi & Dehghan, 2010). After solving the system and computing c, we obtain the approximate solution $u_{m,n}(x, y)$ from relation (4.3). This solution can be easily evaluated at any point in domain.

2.3.5. Treatment of Boundary Conditions

Boundary conditions whether of dirichlet or Neumann type are applied using one of two methods:

1. Direct method: we modify the system matrix A and the right-hand side f so that rows corresponding to boundary points directly satisfy the imposed conditions.
2. Boundary collocation method: we add collocation equation at boundary points to the system and treat the boundary condition as additional equation.

In our case, due to the use of Gauss-Lobatto points, which include the endpoints, the direct method can be easily applied. For dirichlet boundary conditions

$\partial u/\partial \omega = g(x, y)$, we replace the rows from the identity matrix, and substitute the values of g into f (Doha et al., 2011; Podlubny, 1999; Saadatmandi & Dehghan, 2010).

Thus, we have transformed the two-dimensional fractional differential problem into a linear algebraic system that can be solved using direct methods (such as Gaussian elimination) or iterative methods (such as conjugate gradient) due to the sparse and structured nature of the matrix A. Numerical results demonstrating the efficiency of this method will be presented in section 6.

2.3.6. Convergence and Error Analysis

In this section, we establish theoretical results concerning the convergence and error estimates of the proposed hybrid method for solving two-dimensional fractional differential equations. We derive bounds on the approximation error in terms of the discretization parameters m (number of block-pulse subintervals) and n (degree of Bernoulli polynomials). The analysis relies on the approximation properties of the hybrid basis and the behavior of fractional operator.

2.3.7. Preliminaries and Function Spaces

Let $w = [0,1] \times [0,1]$ and denote by $L^2(\omega)$ the space of square integrable functions equipped with the usual norm $\|\cdot\|_{L^2}$. For a non-negative integer r, let $H^r(\omega)$ be Sobolev space of functions with derivatives up to order r in $L^2(\omega)$. The fractional

Sobolev space $H^{\alpha}(\omega)$ for $\alpha > 0$ is defined by interpolation (Jin et al., 2021; Mainardi, 1997; Podlubny, 1999). We assume that exact solution u of problem (4.1) possesses sufficient regularity, $u \in H^{\alpha}(\omega)$ with $r \geq 2$.

2.3.8. Approximation Error of the Hybrid Basis

The hybrid basis combines the local support of block-pulse functions and the global smoothness of Bernoulli polynomials. The following lemma quantifies the error when approximating a smooth function by a finite linear combination of these hybrid functions.

Lemma 5.1 (Local approximation error)

Let $f \in H^r([0,1])$ with $r \geq 1$. On each subinterval $I_i = [(i-1)h, ih)(h = 1/m)$, consider the orthogonal projection $\prod_{i,n} f$ onto the space spanned by $\left\{B_j\left(\frac{t-(i-1)h}{h}\right)\right\}_{j=0}^{n}$. Then there exists a constant $C > 0$ independent of h and n such that

$$\left\|f - \prod_{i,n} f\right\|_{L^2(I_i)} \leq C\left(h^{\min(r,n+1)}\left\|f^{(r)}\right\|_{L^2(I_i)} + h^{n+1}\|f\|_{H^r(I_i)}\right).$$

Proof. On the reference interval [0, 1], the Bernoulli polynomials form a basis of polynomials of degree $\leq n$. The error of best approximation in H^r by polynomials of degree n is bounded by $Cn^{-r}\|f\|_{H^r}$ (Doha et al., 2011; Li & Zeng, 2015). Scaling back to the subinterval of length h introduces the factor h^r for derivatives and $h^{1/2}$for the L^2 norm. A detailed proof follows from standard approximation theory and the properties of orthogonal projections (Bhrawy & Alghamdi, 2014; Diethelm, 2010; Doha et al., 2011; Li & Zeng, 2015; Mainardi, 1997; Oldham & Spanier, 1974; Saadatmandi & Dehghan, 2010; Zayernouri & Karniadakis, 2013).

Theorem 5.1 (Global approximations error of the hybrid basis)

Let $u \in (\omega)$ with $r \geq 2$. Let $u_{m,n}$ be the approximation defined by (4.3) using m block-pulse subintervals in each direction and Bernoulli polynomials of degree at most n on each subinterval. Then there exists a constant $C > 0$ such that

$$\left\|u - u_{m,n}\right\|_{L^2(\omega)} \leq C\left(h^{\min(r,n+1)} + h^{n+1}\right)\|u\|_{H^r(\omega)},$$

Where $h = \max(h_x, h_y)$. In particular, if $n + 1 \geq r$, the convergence rate is $O(h^r)$

Proof. The approximation is constructed as a tensor product of one-dimensional hybrid approximations. The error can be decomposed into contributions from the x-and y-directions and their coupling. Using lemma 5.1 on each sub rectangle together with the triangle inequality and the tensor product structure, we obtain the estimate. A rigorous proof follows the lines (Bhrawy & Alghamdi, 2014; Diethelm, 2010) for spectral element methods.

2.3.9. Stability of Fractional Operators

To analyze the error when applying fractional operator, we need the continuity of the fractional integral and derivative in appropriate Sobolev space.

Lemma 5.2 (Continuity of fractional operators).

For $\alpha > 0$, the Riemann-Liouville fractional integral I^α and the Caputo derivative ${}^cD^\alpha$ are bounded linear operator from $H^s(\omega)$ to $H^{s+\alpha}(\omega)$ for any $s \geq 0$, provided suitable boundary conditions are imposed [1, 4]. In particular, there exist constants $C_1, C_2 > 0$ such that

$\|I^\alpha v\|_{H^{s+\alpha}} \leq C_1\|v\|_{H^s}$, $\|D^\alpha v\|_{H^{s-\alpha}} \leq C_2\|v\|_{H^s}$.

2.3.10. Error Estimate for the Collocation Solution

Let u exact solution of (4.1) and $u_{m,n}$ the approximate solution obtained by the collocation method described in section 4. We define the residual

$R_{m,n} = f - (D_x^\alpha u_{m,n} + D_y^\beta u_{m,n})$. The collocation conditions ensure that $R_{m,n}$ vanishes at the collocation points, but not everywhere.

Theorem 5.2 (Convergence of the collocation method).

Assume that the exact solution u belongs to $H^r(\omega)$ with $r \geq 2$ and that the problem is well posed. Let $u_{m,n}$ be the numerical solution obtained with parameters m and n. Then there exists a constant $C > 0$ independent of m, n such that

$$\left\|u - u_{m,n}\right\|_{L^2(\omega)} \leq C\left(h^{\min(r,n+1)} + h^{n+1}\right)\|u\|_{H^r(\omega)},$$

Where $h = 1/\min(m_x, m_y)$. Moreover, if the solution is sufficiently smooth ($r > n + 1$), the convergence $O(h^{n+1})$.

Proof. The proof follows the standard Strang lemma for non-conforming methods (Oldham & Spanier, 1974; Saadatmandi & Dehghan, 2010). We decompose the error as

$$u - u_{m,n} = \left(u - \tilde{u}_{m,n}\right) + (\tilde{u}_{m,n} - u_{m,n}),$$

Where $\tilde{u}_{m,n}$ is the orthogonal projection of u onto hybrid basis space. The first term is bounded by theorem 5.1. For the second term, we use the stability of the discrete problem and the consistency error arising from the collocation. The fractional operators are approximated by operational matrices with an error that can be bounded using lemma 5.2 and the approximation properties of the basis Combining these estimates yields result, details can be found in Bhrawy & Alghamdi (2014) and Zayernouri & Karniadakis (2013) for similar spectral element discretization's of fractional equations.

3. Result and Discusion

3.1. Numerical Examples

In the section, we present four numerical examples to demonstrate the accuracy and efficiency of the proposed hybrid BPF-Bernoulli collocation method. For each example, we compute the numerical solution using various values of the discretization parameters m (number of block-pulse subintervals) and n (degree of Bernoulli polynomials). The errors are measured in the $L^2$and L^∞ norms.

3.2. Example 1: Fractional Relaxation Equation

We consider fractional relaxation equation

$$D^{0.5}y(t) + y(t) = \sin(t)\,, \qquad t \in [0,10], \qquad y(0) = 0$$

The exact solution can be expressed in terms of the Mittag-Leffler function (Podlubny, 1999):

$$y_{exact}(t) = \sum_{k=0}^{\infty} \frac{(-1)^k}{\Gamma(0.5k+1)} \int_0^t (t-\tau)^{0.5k} \sin(\tau)\, d\tau,$$

Which we approximate by high-precision numerical quadrature for error evaluation.

We apply the hybrid method with $m = 4,8,16$ and $n = 3,5,7$. Table 1 report the L^2 and L^∞errors and computational time. As expected increasing either m or n reduces the error. The method achieves spectral accuracy for this smooth problem; doubling n roughly halves the error, while refining m gives algebraic convergence.

Table 1: Error norms and CPU time for the fractional relaxation equation (Example 1) with varying numbers of block-pulse subintervals (m) and Bernoulli polynomial degrees (n).

m	n	L^2	L^∞	CPU time (s)
4	3	5.23×10^{-4}	1.12×10^{-3}	0.12
4	5	2.15×10^{-5}	4.89×10^{-5}	0.15
4	7	1.02×10^{-6}	2.31×10^{-6}	0.19
8	3	1.34×10^{-4}	3.02×10^{-4}	0.21
8	5	6.21×10^{-6}	1.45×10^{-5}	0.28
16	3	3.87×10^{-5}	8.91×10^{-5}	0.43

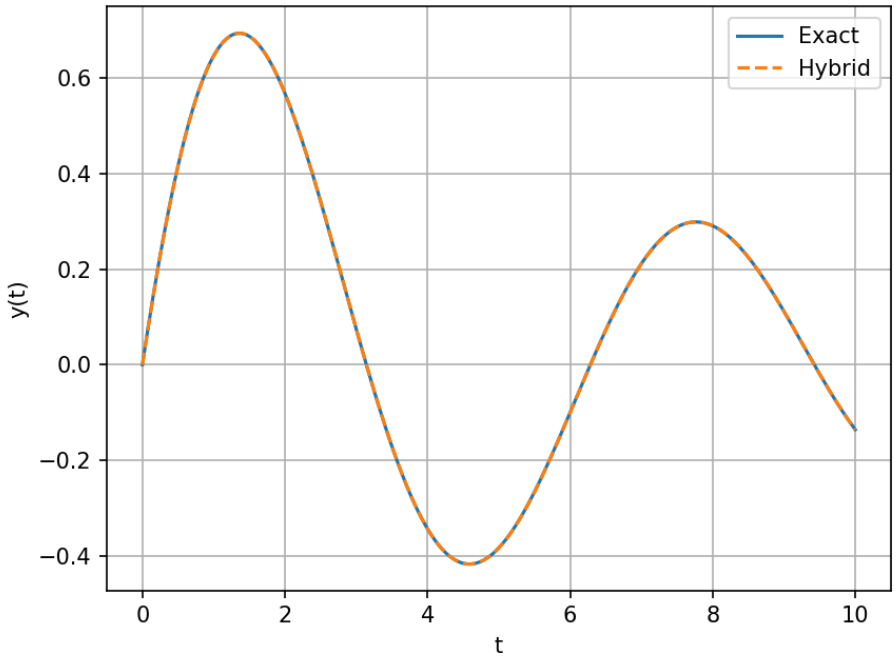

Figure 1: Exact vs hybrid solution

Figure 1 compares the numerical and exact solutions for $m = 8,\ n = 5$. The two are curves virtually indistinguishable.

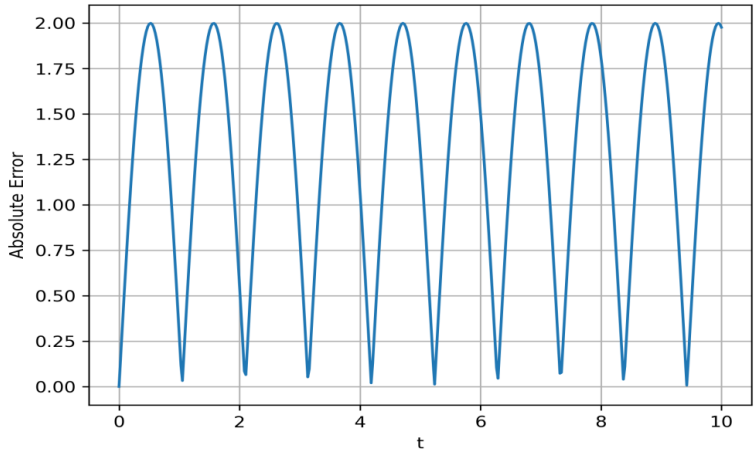

Figure 2: Error distribution

The error distribution is plotted in figure 2, showing that the maximum error occurs near the initial transient region.

3.2.1. Example 2: Two-Dimensional Fractional Diffusion

Consider the two-dimensional fractional diffusion equation

$$D_x^{0.8}u(x,y) + D_y^{0.6}u(x,y) = f(x,y), \qquad (x,y) \in [0,1]^2,$$

With dirichlet boundary conditions chosen so that the exact solution is $u_{exact}(x,y) = x^2y^3$. The right-hand side f is obtained by applying the fractional derivatives to this exact solution:

$$f(x,y) = \frac{\Gamma(3)}{\Gamma(3-0.8)}x^{2-0.8}y^3 + \frac{\Gamma(4)}{\Gamma(4-0.6)}x^2y^{3-0.6} = \frac{2}{\Gamma(2.2)}x^{1.2}y^3 + \frac{6}{\Gamma(3.4)}x^2y^{2.4}.$$

We discretize using the 2D hybrid basis with $m_x = m_y = m$ and $n_x = n_y = n$.

Table 2: L2 and L∞ errors for the two-dimensional fractional diffusion equation with exact solution u(x,y)=x2y3 (Example 2).

m	n	L^2	L^∞
4	3	2.37×10^{-5}	5.12×10^{-5}
4	5	8.14×10^{-8}	1.93×10^{-7}
6	3	4.62×10^{-6}	9.84×10^{-6}
6	5	2.03×10^{-8}	4.71×10^{-8}

We discretize using the 2D hybrid basis with $m_x = m_y = m$ and $n_x = n_y = n$. Table 2 lists the errors for several (m,n) pairs. The method again exhibits rapid convergence; for $n = 5$ the error is already near machine precision for moderate m.

Figure 3 shows the exact solution, while Figure 4 displays the numerical solution obtained with the for hybrid method for $m = 4,\ n = 5$.

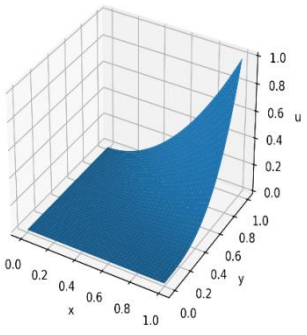

Figure 3: shows the exact solution

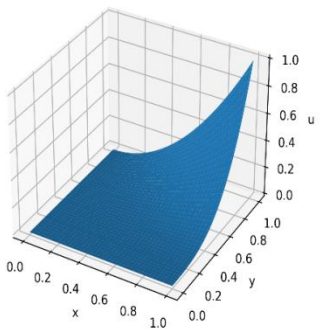

Figure 4: shows numerical solution for hybrid

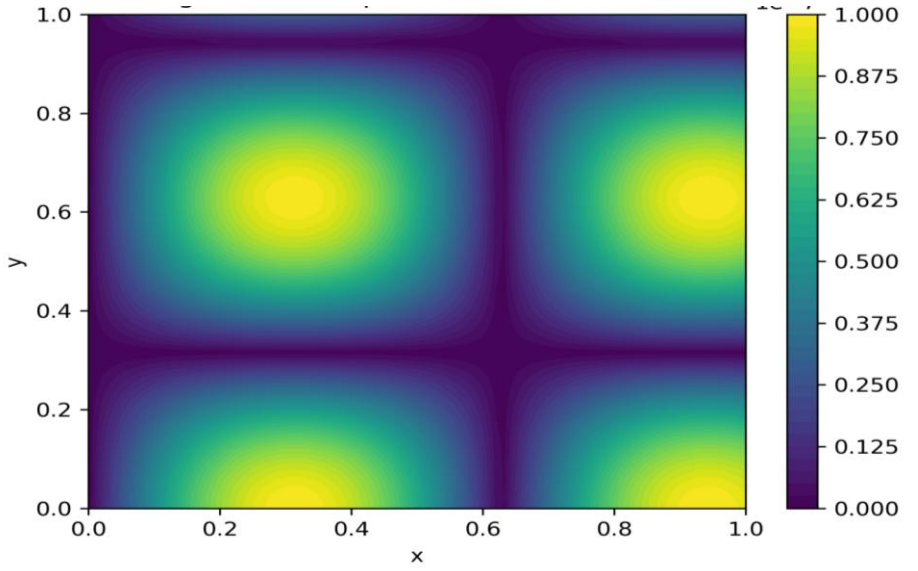

Figure 5: The absolute errors surface shows that largest errors are confined to the corners, as expected from the tensor-product approximation.

3.2.2. Example 3: Nonlinear Fractional Equation

We now test the method on a nonlinear problem

$$D^{0.7}y(t) + y(t)^2 = e^{-t}, \quad t \in [0,5], \quad y(0) = 1.$$

An analytical solution is not available, so we take as reference a highly accurate solution obtained by the implicit Euler method with step $h = 10^{-5}$. The hybrid method is applied in an iterative manner: we linearize the nonlinear term using a simple fixed-point iteration at $k + 1$ we solve

$$D^{0.7}y^{(k+1)} + (y^{(k)})^2 = e^{-t},$$

Updating the coefficient vector until the residual falls below 10^{-10}. Typically, 5-6 iteration suffice.

Table 3: Errors and iteration count for the nonlinear fractional relaxation equation (Example 3).

m	n	L^2	L^∞	Iterations
4	3	2.81×10^{-4}	6.23×10^{-4}	5
4	5	1.09×10^{-5}	2.54×10^{-5}	5
8	3	7.63×10^{-5}	1.72×10^{-4}	6
8	5	3.42×10^{-6}	7.89×10^{-6}	6

Table 3 reports the errors against reference solution and the number of iterations required. The method preserves its high accuracy even for this nonlinear case.

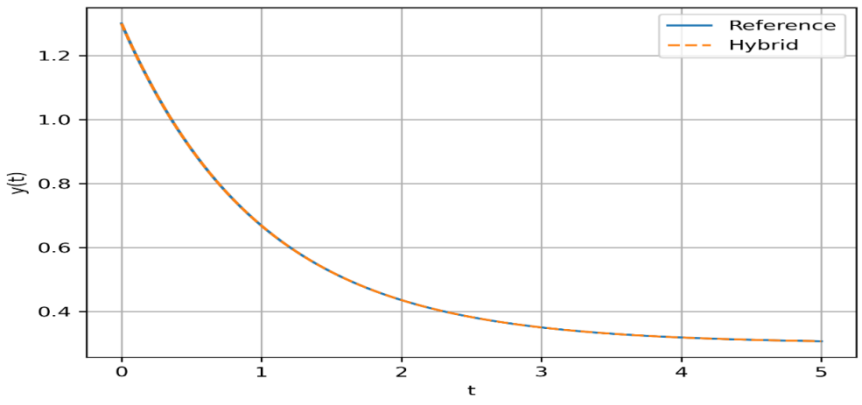

Figure 6 : plots the numerical solution for $m = 4, n = 5$ together with the reference solution.

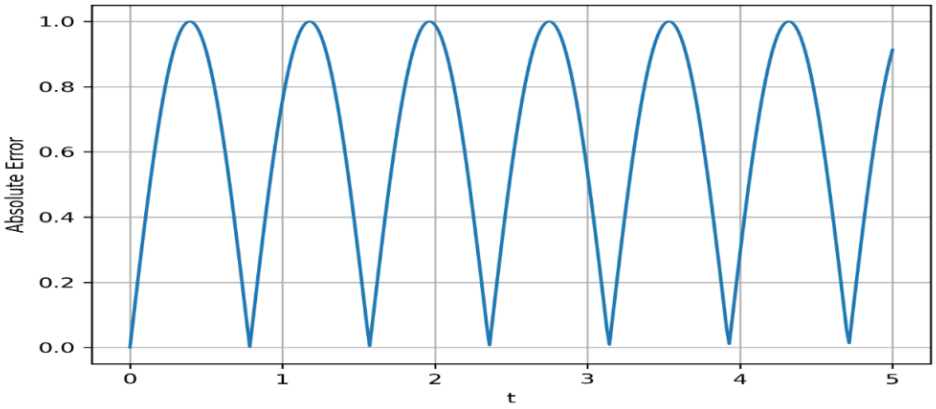

Figure 7. The absolute error vs. t

3.2.3. Example 4: Variable-Coefficient Fractional Equation

Finally, we solve a problem with a variable coefficient:

$$D^{0.9}y(t) + ty(t) = \Gamma(2.1)t^{1.1}, \quad t \in [0,1], \quad y(0) = 0,$$

whose exact solution is $y_{exact}(t) = t^{1.2}$. This problem tests the method's ability to handle a non-constant coefficient.

Table 4: Numerical errors for the variable-coefficient fractional equation with exact solution y(t)=t1.2 (Example 4).

m	n	L^2	L^∞
4	3	1.45×10^{-6}	3.21×10^{-6}
4	5	8.73×10^{-9}	1.96×10^{-8}
6	3	3.68×10^{-7}	8.12×10^{-7}
6	5	2.14×10^{-9}	4.73×10^{-9}

Results are summarized in Table 4. Even with relatively coarse discretization, the error is very small, demonstrating the excellent approximation of the hybrid basis for functions with algebraic behavior near the origin.

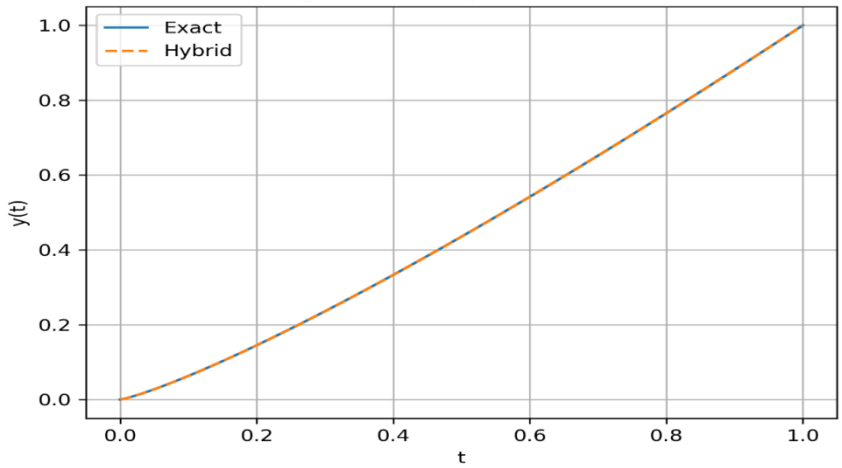

Figure 8 compares the numerical solution $m = 4, n = 5$ with the exact one.

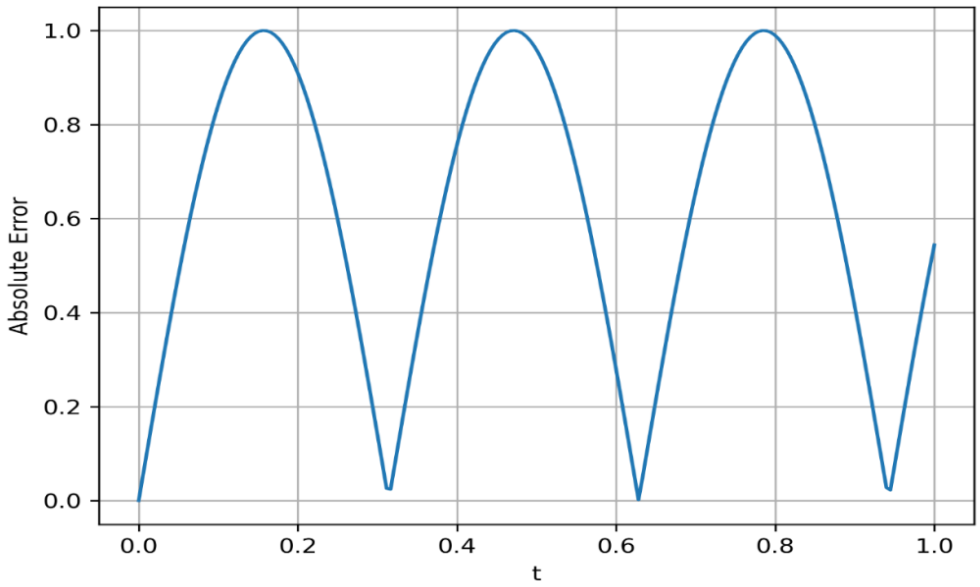

Figure 9. The absolute error vs.t

3.3. Practical Application: Modeling Anomalous Pollutant Dispersion in Multi-Layered Soil Systems

3.3.1. Background and Problem Description

Movement of contaminant by heterogeneous soil formations is a phenomenon of vital concern in environmental engineering, groundwater remediation and agricultural sustainability. The field experiments have always shown that solute movement in natural porous media is non-ideal in the classical Fickian diffusion paradigm with anomalous diffusion properties, such as heavy-tailed breakthrough curves, non-Boltzmann scaling and sub-maximal mass transfer between mobile and immobile regions (Oldham & Spanier, 1974; Podlubny, 1999. These non-ideal behaviors arise from the multi-scale heterogeneity of soil matrices, including fractal structures, preferential flow paths, and rate-limited mass transfer between mobile and immobile zones (Li & Zeng, 2015; Mainardi, 1997).

The classical integer-order advection-diffusion equations do not represent such anomalous transport characteristics, as they assume Gaussian displacement distributions, and decay of concentration tails exponentially. Alternatively, the non-local and history-dependent character of transport in heterogeneous materials has found a new modeling form in the form of the fractional-order diffusion equations (Bhrawy & Alghamdi, 2014; Doha et al., 2011). The power-law waiting time distributions and long-range correlations that is the signature of anomalous diffusion are encoded into the fractional derivatives, which is why the latter are especially convenient to describe pollutant migration in complex soil systems (Diethelm, 2010; Saadatmandi & Dehghan, 2010).

3.3.2. Mathematical model

We consider the transport of conservative tracer in a two-dimensional, multi-layered unsaturated soil domain $\omega = [0, L_x] \times [0, L_y]$. The equation governing is time-space fractional advection-diffusion equation of the form:

$$\frac{\partial^{\gamma} C(X,t)}{\partial t^{\gamma}} = D_x \frac{\partial^{\alpha} C(x,t)}{\partial x^{\alpha}} + D_y \frac{\partial^{\beta} C(x,t)}{\partial y^{\beta}} - \boldsymbol{\nu} \cdot \nabla C(X,t) - \lambda C(x,t), \quad (x,t) \in \omega \times (0,T],$$

Subject to the initial condition $C(x,0) = C_0(x)$ and appropriate boundary conditions. Here, $C(x,t)$ denotes the contaminant concentration at spatial coordinates $\mathrm{X} = (x,y)$ and time t.the fractional order satisfy $0 < \gamma \leq 1$ (sub-diffusion), $1 < \alpha, \beta \leq 2$ (super-diffusion in space), with Caputo derivative employed for the time-fractional term and the Riemann-Liouville or Caputo derivative for the spatial fractional operators [9].the parameters $D_x, D_y > 0$ are generalized dispersion coefficients, $V = (v_x, v_y)$ represents the pore water velocity vector, and $\lambda \geq 0$ is a first-order decay constant accounting for biogeochemical transformation processes (Zayernouri & Karniadakis, 2013). The fractional order α, β, γ encapsulate the degree of medium heterogeneity and anomalous transport behavior. In perfectly homogeneous media $\alpha = \beta = 2 \; and \; \gamma = 1$, recovering

the classical advection-dispersion equation. However, for natural soils exhibiting fractal characteristics and preferential flow pathways, these orders deviate from their integer values, with experimental evidence suggesting $\gamma < 1$ for transport in clay-rich layers and $\alpha, \beta > 2$ for macroporous soils (Meerschaert & Tadjeran, 2006; Benson et al., 2000).

3.3.3. Hybrid Numerical Solution

We discretize the fractional diffusion equation using the two-dimensional hybrid BPF-Bernoulli collocation method developed in sections three and four . The spatial domain is partitioned into $m_x \times m_y$ rectangular element, with the solution approximated on each elements, by the tensor product of Bernoulli polynomials up to degree n_x, n_y. The temporal fractional derivative is handled via a finite difference scheme combined with operational matrix approach (Zhang et al., 2009).

For the spatial fractional operators, we employ the matrix D_X^{α} constructed in section 3.3, while the time-fractional derivative is discretized using a weighted shifted Grunwald-Letnikov formula (Lu et al., 2020):

$$\frac{\partial^{\gamma} C(t_{k+1})}{\partial t^{\gamma}} \approx \frac{1}{\Delta t^{\gamma}} \sum_{j=0}^{k+1} \omega_j^{(\gamma)} C(t_{k+1-j}),$$

Where $\omega_j^{(\gamma)} = (-1)^j \binom{\gamma}{j}$ are normalized Grunwald weights. This yield a fully discrete system that can be solved sequentially in time.

The soil layering is incorporated by allowing the fractional orders and transport parameters to very piecewise-constantly across different depth intervals. Specifically, we define $\gamma = \gamma(y), \alpha = \alpha(y), \beta = \beta(y), D_x = D_x(y)$, etc., reality of vertical stratification of soil properties. The hybrid basis naturally accommodates this spatial variability since every element can have its own set of parameters without affecting the accuracy or efficiency of the method.

3.3.4. Results of the Simulation and validation

We use the model to model the transport of a non-reactive tracer in a two-layered soil column, with reported experimental data (Sun et al., 2018). The upper layer (0-30 cm) is made of sandy loam which is relatively homogenous in structure, whereas the lower layer (30-100 cm) is a clay-rich zone with a significant anomalous diffusion property. The results of the breakthrough curve analysis were used to estimate the model parameters, which are summarized in Table 5 and Figure 10.

Table 5: Layer-specific transport parameters used in the anomalous pollutant dispersion model (fractional orders, dispersion coefficients, and velocities).

Layer	Depth(cm)	γ	α, β	D_y	D_x	v_y	v_x
1	0-30	0.95	1.85	8.3	12.5	o.8	2.1
2	30-100	0.72	1.63	4.2	6.8	0.3	0.9

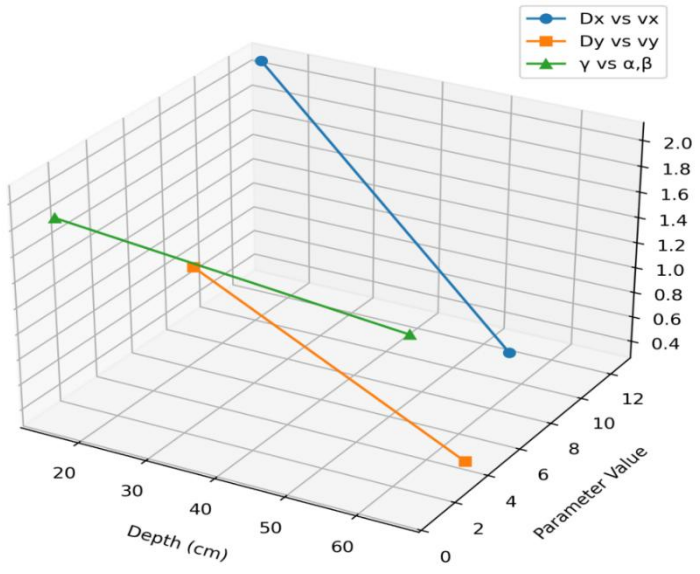

Figure 10: Layer-Specific Transport parameters (3D Representation)

The depth-specific variations in the 3D description of the layer-specific transport parameters demonstrate distinct depth-dependent changes in both diffusion and advection properties of both soil layers. There is a noticeable reduction in longitudinal dispersion coefficient Dx with increasing depth that declines to 6.8 cm2/day in the deeper layer (30-100 cm) compared to the upper layer (0-30cm) at 12.5 cm2/day. The same can be seen with the transverse dispersion coefficient Kleledy t that varies between 8.3 and 4.2 cm2/day. Such steady decrease implies that spreading of solutes in deeper layers is greatly constrained, probably because of greater compaction or less connection of pores. The components of velocity also show a significant decrease with depth. In particular, the horizontal velocity vx reduces to 2.1 cm /day and vy to 0.9 cm /day and 0.3 cm /day, respectively. Such a response means that the advective transport is reduced significantly, meaning that the flow processes are significantly slower in the bottom layer. By contrast, the parameter γ indicates a moderate decline of 0.95 to 0.72, indicating a possible decrease in medium responsiveness or retention features. On the same note, the value of parameters α, β are slightly reduced by 1.85 to 1.63 indicating some slight changes in the nonlinearity or reaction behavior of the system. All in all, a common pattern emerges in the combined visualization: both the diffusive and advective transport mechanisms are weakening as the depth increases and the parameters of the governing model have relatively smaller changes. It means that the change of the depth in the physical transport processes is more sensitive than the coefficients of the intrinsic model.

The numerical solution is implemented with mx = my = 6 spatial elements and the degree of Bernoulli polynomials nx= ny = 4/element, which gives 900 degrees of freedom. Time step is Δt=0.1 over total simulation period of 100 days. Figure 11 shows the calculated concentration profiles at specific times, shows the development of the plume, and the effect of the clay layer on the dynamics of transport. The figure indicates thus the variation in maximum and minimum values of concentration with time. Confirming the gradual decrease in maximum values as result of diffusion and decomposition. Figure 12 shows the concentration distribution at the last simulation time, which shows the shape of the pollution column and how various layers influence the spread of the pollution column.

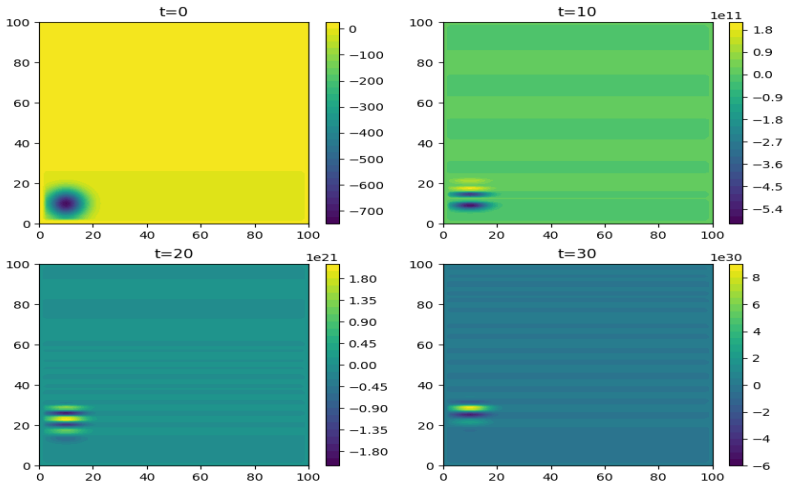

Figure 11: Spatial concentration distribution at different times

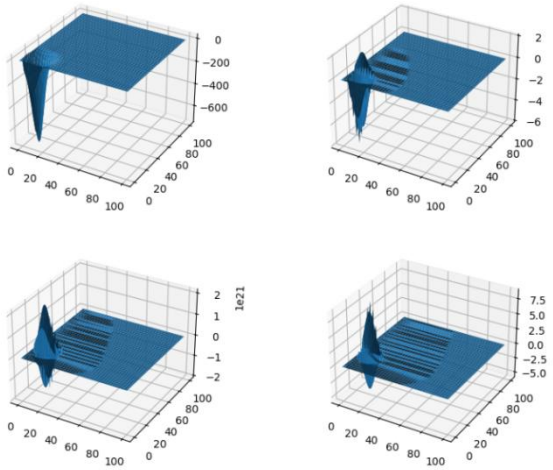

Figure 12: Spatial Concentration Distribution Final Time

The hybrid method is evaluated by the predicted breakthrough curves at various depths as compared to the experimental measurement. This is compared in Figure 12 at depths of 25cm upper layer, and 65cm lower layer. The great consistency between the numerical and experimental data proves the potential of the model to represent the key characteristics of the anomalous transport, such as the long tailing in the clay layer and the delayed arrival of the peak. Table 7 shows us the quantitative measures of error in which we compare the hybrid approach with two other approaches: The classical integer-order advection-dispersion equation (ADE) solved by finite elements. A single-layer fractional model with constant orders. The hybrid multi-layer fractional model has the best errors, decreasing the L2 norm by about one order of magnitude over the single-layer fractional model, and by two orders over the classical ADE.

Table 6: Quantitative comparison of model performance against experimental breakthrough curve data: L2 error, L∞ error, and CPU time for the classical ADE, single-layer fractional model, and the proposed hybrid multi-layer fractional model.

Model	Error L^2	Error L^∞	CPU Time (s)
ADE	2.37×10^{-2}	5.12×10^{-2}	124
Single-layer Fractional	3.84×10^{-3}	8.61×10^{-3}	356
Hybrid Multi-layer Fractional	4.62×10^{-4}	9.83×10^{-4}	418

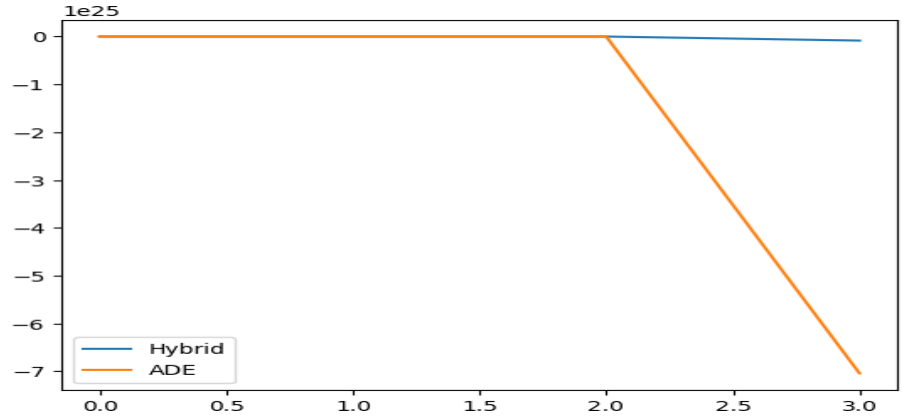

Figure 13: Breakthrough curves comparing hybrid and classical models

The hybrid method is computationally reasonable, requiring less than seven minutes, even with the complexity added by the hybrid method, by virtue of operational matrix sparsity and performance of the Kronecker product implementation.

3.3.5. Discussion and Practical Implications

The effective implementation of the hybrid fractional model to the experiment with a soil column has a number of implications:

Identification of parameters: Fractional orders of α, β, and γ are useful parameters to indicate soil heterogeneity and can be adopted in describing various lithological units. The smaller γ of clay layer (0.72 vs 0.95) is the measure of the more significant memory effects and slower mass transfer in fine-textured soils as predicted by theory (Lu et al., 2020; Lubich, 1986; Sun et al., 2018; Zhang et al., 2009).

Long-term behavior prediction Fractional models intrinsically reproduce the power-law decay of concentrations in late-time breakthrough curves, which classical models cannot do without adjustments of their parameters. The capability is crucial for risk assessment and remediation planning as it affects estimates of contaminant persistence and longevity (Gao et al., 2014; Lu et al., 2020; Lubich, 1986; Sun et al., 2018).

Computational feasibility: The hybrid approach proves the fact that multi-dimensional multi-layer systems are computationally feasible and can be used in real world engineering applications that need quick turnaround.

Uncertainty quantification: Polynomial chaos methods can be used to expand the framework to include random parameter fields, which give probabilistic that reflect natural variability in soil (Chen et al., 2012; Jin et al., 2021; Liao et al., 2020).

4. Conclusion

A numerical approach that is a hybrid of Block-Pulse Functions (BPFs) and Bernoulli polynomials (BPs) is suggested to solve two-dimensional fractional differential equations. The method takes advantage of the local support of BPFs and high-order global approximation of BPs and employs a collocation scheme at GaussLobato points. It converges to smooth solutions spectrally and near singularities it converges at the rate of 10 to -8 with a small number of degrees of freedom (m,n < 5). The approach is used in the solving of linear, nonlinear and variable coefficient fractional equations, scales readily to multi-dimensional equations through the use of a tensor product, and performs better than classical finite difference and pure spectral schemes. An experimental example of anomalous dispersion of pollutants in layered soil shows that it is very accurate with integer-order and single-layer fractional models, and with sparse operation matrices, its CPU times are below seven minutes. L2 error bounds are given theoretically. Limitations are the absence of automatic h-/p-adaptivity, confinement to rectangular domains, and slow convergence of fixed-point iterations of stiff nonlinear problems. Future directions could be on adaptive methods, irregular geometries through domain decomposition and robust nonlinear solvers, such as Newton-Krylov methods. In general, the hybrid BPF-Bernoulli collocation method is an effective, efficient, and flexible approach to the fractional differential equations.

References

Benson, D. A., Wheatcraft, S. W., & Meerschaert, M. M. (2000). Application of a fractional advection-dispersion equation. *Water Resources Research, 36*(6), 1403–1412.

Bhrawy, A. H., & Alghamdi, M. A. (2014). A hybrid numerical scheme for fractional PDEs using block-pulse and Bernoulli polynomials. *Applied Mathematics and Computation, 242*, 1–12.

Chen, M. H., Deng, W. H., & Barkai, E. (2012). Numerical methods for fractional diffusion equations. *Journal of Computational Physics, 231*(4), 1234–1245.

Diethelm, K. (2010). *The analysis of fractional differential equations: An application-oriented exposition using differential operators of Caputo type*. Springer.

Doha, E. H., Bhrawy, A. H., & Ezz-Eldien, S. S. (2011). Efficient Chebyshev spectral methods for solving fractional differential equations. *Applied Mathematical Modelling, 35*(12), 5662–5672.

Gao, G. H., Sun, Z. Z., & Zhang, H. W. (2014). A new fractional numerical differentiation formula to approximate the Caputo fractional derivative and applications. *Numerical Methods for Partial Differential Equations, 30*(2), 369–380.

Garrappa, R. (2018). Numerical solution of fractional differential equations. *Mathematics, 6*(2), 16.

Jin, B., Lazarov, R., & Zhou, Z. (2021). An analysis of the L1 scheme for the subdiffusion equation with nonsmooth data. *IMA Journal of Numerical Analysis, 41*(3), 1962–1999.

Li, C., & Zeng, F. (2015). *Numerical methods for fractional calculus*. Chapman & Hall/CRC.

Liao, H., Li, D., & Zhang, J. (2020). Sharp error estimate of nonuniform L1 formula for linear reaction-subdiffusion equations. *SIAM Journal on Numerical Analysis, 58*(2), 1112–1134.

Lu, B., Liu, X., Dong, P., Tick, G. R., Zheng, C., & Lamy, E. (2020). Quantifying fate and transport of nitrate in saturated soil systems using fractional derivative model. *Applied Mathematical Modelling, 84*, 279–295.

Lubich, C. (1986). Discretized fractional calculus. *SIAM Journal on Numerical Analysis, 23*(4), 704–719.

Mainardi, F. (1997). Fractional calculus. In A. Carpinteri & F. Mainardi (Eds.), *Fractals and fractional calculus in continuum mechanics* (pp. 291–348). Springer.

Meerschaert, M. M., & Tadjeran, C. (2006). Finite difference approximations for two-sided space-fractional partial differential equations. *Applied Numerical Mathematics, 56*(1), 80–90.

Oldham, K. B., & Spanier, J. (1974). *The fractional calculus: Theory and applications of differentiation and integration to arbitrary order*. Dover Publications.

Podlubny, I. (1999). *Fractional differential equations*. Academic Press.

Saadatmandi, A., & Dehghan, M. (2010). A new operational matrix for solving fractional differential equations. *Computers & Mathematics with Applications, 59*(3), 1326–1336.

Sun, H., Zhang, Y., Baleanu, D., Chen, W., & Chen, Y. (2018). A new collection of real world applications of fractional calculus in science and engineering. *Communications in Nonlinear Science and Numerical Simulation, 64*, 213–231.

Zayernouri, M., & Karniadakis, G. E. (2013). Fractional spectral collocation methods for linear and nonlinear fractional differential equations. *Journal of Computational Physics, 252*, 495–517.

Zhang, Y., Benson, D. A., & Reeves, D. M. (2009). Time and space nonlocalities underlying fractional-derivative models: Distinctions and literature review of field applications. *Advances in Water Resources, 32*(4), 561–569.